

AD-A236 032



2



PL-TR-91-3012

AD:

Final Report
for the period
August 1990 to
January 1991

ABSOLUTE CONCENTRATION MEASUREMENTS OF FREE RADICALS IN FLAMES BY ABSORPTION SPECTROSCOPY

April 1991

Authors:
S. Zabarnick
D.A. Alspach



Approved for Public Release

Distribution is unlimited. The OL-AC PL Technical Services Office has reviewed this report and it is releaseable to the National Technical Information Service, where it will be available to the general public, including foreign nationals.

Phillips Laboratory

Air Force Systems Command
Propulsion Directorate
Edwards AFB CA 93523-5000



91 5 28 013

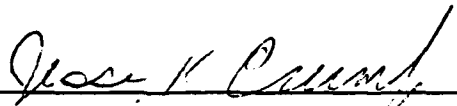
NOTICE

When U.S. Government drawings, specifications, or other data are used for any purpose other than a definitely related Government procurement operation, the fact that the Government may have formulated, furnished, or in any way supplied the said drawings, specifications, or other data, is not to be regarded by implication or otherwise, or in any way licensing the holder or any other person or corporation, or conveying any rights or permission to manufacture, use or sell any patented invention that may be related thereto.

FOREWORD

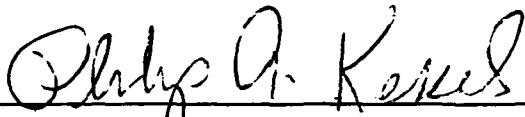
This interim report was submitted on completion of this phase of JON: 2308M1Q2 by the OL-AC PL/RKFT Branch, at the Phillips Laboratory (AFSC) (formerly Astronautics Laboratory), Edwards AFB CA 93523-5000. OL-AC PL Project Manager was Capt Jesse Crump.

This report has been reviewed and is approved for release and distribution in accordance with the distribution statement on the cover and on the DD Form 1473.



JESSE K. CRUMP, CAPT, USAF
Project Manager

FOR THE COMMANDER



PHILIP A. KESSEL
Chief, Thermophysics Branch



DAVID LEWIS, MAJ, USAF
Acting Director
Fundamental Technologies Division

REPORT DOCUMENTATION PAGE

Form Approved
OMB No. 0704-0188

a. REPORT SECURITY CLASSIFICATION Unclassified		1b. RESTRICTIVE MARKINGS	
a. SECURITY CLASSIFICATION AUTHORITY		3. DISTRIBUTION/AVAILABILITY OF REPORT Approved for public release; Distribution is unlimited.	
b. DECLASSIFICATION/DOWNGRADING SCHEDULE		5. MONITORING ORGANIZATION REPORT NUMBER(S)	
4. PERFORMING ORGANIZATION REPORT NUMBER(S) PL-TR-91-3012		7a. NAME OF MONITORING ORGANIZATION	
5a. NAME OF PERFORMING ORGANIZATION Phillips Laboratory	6b. OFFICE SYMBOL (If applicable) RKFT	7b. ADDRESS (City, State, and ZIP Code)	
8c. ADDRESS (City, State, and ZIP Code) OL-AC, PL/RKFT Edwards AFB CA 93523-5000		9. PROCUREMENT INSTRUMENT IDENTIFICATION NUMBER	
9a. NAME OF FUNDING/SPONSORING ORGANIZATION	8b. OFFICE SYMBOL (If applicable)	10. SOURCE OF FUNDING NUMBERS	
8c. ADDRESS (City, State, and ZIP Code)		PROGRAM ELEMENT NO. 61102F	PROJECT NO. 2308
		TASK NO. MI	WORK UNIT ACCESSION NO. Q2
11. TITLE (Include Security Classification) Absolute Concentration Measurements of Free Radicals in Flames by Absorption Spectroscopy			
12. PERSONAL AUTHOR(S) S. Zabarnick, D. A. Alspach			
13a. TYPE OF REPORT Interim	13b. TIME COVERED FROM 90/8 TO 91/1	14. DATE OF REPORT (Year, Month, Day) 91/04	15. PAGE COUNT 40
16. SUPPLEMENTARY NOTATION			
17. COSATI CODES		18. SUBJECT TERMS (Continue on reverse if necessary and identify by block number)	
FIELD	GROUP	Combustion Spectroscopy, Chemical Kinetics	
19	07		
19. ABSTRACT (Continue on reverse if necessary and identify by block number) Absorption spectroscopy techniques were used for measurement of absolute concentrations of free radical species in premixed, laminar, flat-flames of CH ₄ /N ₂ O and CH ₄ /NO/O ₂ . Absolute concentration measurements were performed for the species OH, CN, and NH in 63 Torr flames. These absolute concentration measurements were used to calibrate relative concentration profiles taken in previous experiments using laser-induced fluorescence (LIF) spectroscopy. Significant absorptions of these species could be obtained even in the very short path length flames studied. These measurements permit the experimental LIF measurement to be directly compared to the species concentration profiles predicted by the CHEMKIN/PREMIX flames modeling code.			
20. DISTRIBUTION/AVAILABILITY OF ABSTRACT <input checked="" type="checkbox"/> UNCLASSIFIED/UNLIMITED <input type="checkbox"/> SAME AS RPT. <input type="checkbox"/> DTIC USERS		21. ABSTRACT SECURITY CLASSIFICATION Unclassified	
22a. NAME OF RESPONSIBLE INDIVIDUAL Capt Jesse Crump		22b. TELEPHONE (Include Area Code) 805-275-5657	22c. OFFICE SYMBOL OL-AC, PL/RKFT

Table of Contents

<u>Section</u>	<u>Page</u>
Summary	1
Introduction	2
Equipment and Procedures	3
Chamber and Burner	3
Illumination Source, Optics, and Electronics	3
Determination of Photomultiplier Tube Saturation Level	7
Determination of Burner Surface Position	7
Method for Relating Absorption Profiles to Absolute Concentrations	7
Results	15
Emission Spectroscopy	15
OH Emission	15
CN Emission	15
NH Emission	15
Absorption Spectroscopy	15
OH Absorption	15
CN Absorption	16
NH Absorption	16
Conclusions	17
References	24
Appendix A. Listing of Curves of Growth Integration Routine	25
Appendix B. Tabulated Curves of Growth Data	32
Appendix C. Sample Calculation for the OH radical in a CH ₄ /N ₂ O flame	34

List of Figures

<u>Figure</u>	<u>Caption</u>	<u>Page</u>
1	Schematic of Experimental Apparatus for Absorption Studies	5
2	Burner Chamber	6
3	Flat Flame Burner	7
4	Typical Absorption Profile	8
5	Voigt Profiles for Various Values of the Broadening Parameter	11
6	Curves of Growth Plots for Various Values of the Broadening Parameter	12
7	Emission Spectrum for the OH radical from 306 to 310 nm	18
8	Emission Spectrum for the CN radical from 385.5 to 388.5 nm	19
9	Emission Spectrum for the NH radical from 332 to 338 nm	20
10	Absorption Profiles for the Q ₁ (6) transition of OH. Top: CH ₄ /N ₂ O flame; bottom: CH ₄ /NO/O ₂ flame.	21
11	Absorption Profiles for the unresolved R(15) doublet of CN. Top: CH ₄ /N ₂ O flame; bottom: CH ₄ /NO/O ₂ flame.	22
12	Absorption Profiles for the R(8) transitions of NH. Top: R(8) triplet in the CH ₄ /N ₂ O flame; bottom: R ₂ (8) transition.	23

List of Tables

<u>Table</u>	<u>Caption</u>	<u>Page</u>
1	Flame Conditions Employed in Study	3
2	Distance From Burner Surface	3
3	Integrated Areas for OH, CN, and NH Absorption Profiles in CH ₄ /N ₂ O and CH ₄ /NO/O ₂ Flames at 63 Torr	16
4	Absolute Concentrations of OH, CN, and NH in CH ₄ /N ₂ O and CH ₄ /NO/O ₂ Flames at 63 Torr	16

List of Symbols

<u>English Symbols</u>	<u>Description</u>
a	broadening parameter
A_{ω}	spectral absorption
B_v	rotational constant
c	speed of light
e	electronic charge (4.80×10^{-10} esu, esu = $g^{1/2}cm^{3/2}/sec$)
$F(J'')$	rotational energy term for level J''
$f_{v''v'}$	band oscillator strength for the transition from J'' to J'
$G(v)$	vibrational energy term for level v
h	Planck's constant
$I_{\omega}(0)$	spectral intensity before entering absorbing medium
$I_{\omega}(l)$	spectral intensity after traveling path length l through absorbing medium.
J'	rotational quantum number of upper level
J''	rotational quantum number of lower level
K_{ji}	line strength for transition from energy level j to energy level i
$K_{J''J'}$	line strength for transition from J'' to J'
k	Boltzmann constant
k_{ω}	spectral absorption coefficient
l	path length
m_e	electron mass (9.1×10^{-28} g)
N	number density
$N_{J''}$	number density for the lower rotation level J''
Q_e	electronic partition function
Q_r	rotational partition function



Accession For	
NTIS GRA&I	<input checked="" type="checkbox"/>
DTIC TAB	<input type="checkbox"/>
Unannounced	<input type="checkbox"/>
Justification _____	
By _____	
Distribution/ _____	
Availability Codes	
Dist	Avail and/or Special
A-1	

<u>English Symbols</u>	<u>Description</u>
Q_v	vibrational partition function
S	spin quantum number
$S_{J''J'}$	rotational line strength for transition from J'' to J'
$T_e(n)$	electronic term energy
$T_{J''J'}$	correction factor to account for increased inter-nuclear separation at higher rotational quantum numbers in calculating band oscillator strengths
T_ω	spectral transmission
$V(\xi, a)$	Voigt line profile
$W_{J''J'}$	integrated absorption for transition from J'' to J'
$Y(\omega)$	line profile
y	Voigt function parameter

<u>Greek Symbols</u>	<u>Description</u>
ξ	Voigt function parameter
Λ	quantum number for the projection of the total electronic orbital angular momentum on the inter-nuclear axis
ϕ	=1 for $\Lambda=0$ =2 for $\Lambda \neq 0$
$\Delta\omega_D$	Doppler full width at half maximum
ω	wave number
ω_1^*, ω_2^*	spectral line limits

Summary

Absorption spectroscopy techniques were used for measurement of absolute concentrations of free radical species in premixed, laminar, flat-flames of $\text{CH}_4/\text{N}_2\text{O}$ and $\text{CH}_4/\text{NO}/\text{O}_2$. Absolute concentration measurements were performed for the species OH, CN, and NH in 63 Torr flames. These absolute concentration measurements were used to calibrate relative concentration profiles taken in previous experiments using laser-induced fluorescence (LIF) spectroscopy. Significant absorptions of these species could be obtained even in the very short path length flames studied. These measurements permit the experimental LIF measurements to be directly compared to the species concentration profiles predicted by the CHEMKIN/PREMIX flame modeling code.

Introduction

The measurement of radical species concentration is vital in the study of combustion chemistry. These free radicals play a major role in the kinetic mechanism because of their high reactivity. Unfortunately, due to this high reactivity, the very low concentrations of these short-lived species can not be determined using conventional intrusive techniques (e.g., probe sampling). Therefore, non-intrusive techniques such as laser-induced fluorescence (LIF) spectroscopy have become valuable tools in the study of free radicals in combustion and flame chemistry. The LIF technique allows for measurement of relative concentration profiles and absolute temperatures in the hostile combustion environment. One drawback of LIF is its inability to readily measure absolute concentrations of these species.

A useful technique for the measurement of absolute concentrations of free radicals in flames is absorption spectroscopy [Ref. 1]. Absorption spectroscopy is a non-intrusive technique which does not perturb the flame environment. By passing light through a point in the flame and measuring the relative intensity and wavelength of the absorbed light, the absolute number of molecules in the focal volume can be determined. By linking the two techniques and matching the absolute concentration obtained through absorption with the corresponding relative values determined using LIF, the entire LIF profile can be converted into absolute concentrations.

The goal of this study was to develop the techniques to make absolute concentration measurements using absorption spectroscopy, and to perform those measurements in the appropriate flame conditions to support the current LIF work being performed at the laboratory. The flames studied in this experiment were the same flames studied in the LIF experiments: $\text{CH}_4/\text{N}_2\text{O}$ and $\text{CH}_4/\text{NO}/\text{O}_2$ [Ref. 2]. These flames were judiciously chosen because of their chemical relevancy to rocket propellant combustion mechanisms. By studying these "simple" flame systems, the knowledge gained can be applied to more complex combustion systems

The species which were measured in this experiment were OH, CN, and NH. These were chosen specifically to match the species in the LIF study and because there is a fair amount of existing work which uses these radicals on which we could test and calibrate our system. Included in this report are the absolute concentrations measured in the $\text{CH}_4/\text{N}_2\text{O}$ and the $\text{CH}_4/\text{NO}/\text{O}_2$ flames, the emission and absorption profiles measured during this experiment, and a sample calculation for the determination of absolute concentrations from absorption data.

Equipment and Procedures

Chamber and Burner

An overall schematic of the experimental apparatus as used in the absorption studies is shown in Fig. 1. The experiment was conducted at subatmospheric pressures inside the chamber shown in Fig. 2. The chamber is evacuated through an access port in the top plate by a Welch Duo-Seal 1397 mechanical pump (500 lpm pumping speed). The chamber pressure is measured using MKS Baratron capacitance manometers and is regulated by a manual flow valve. Optical access to the chamber is provided by four quartz windows.

The flat-flame, premixed burner used in this experiment is shown in Fig. 3. The burner consists of a 1.9 cm stainless steel tube filled with many 1 mm capillary tubes used to create a laminar flow. The burner is mounted on a three-axis Aerotech ATS 400 Series Positioning Stage Translator assembly controlled by an Aerotech Unidex stage controller. The translation stages are enclosed in a containment vessel attached to the bottom of the chamber as shown in Fig. 1. The translation assembly allows 1 μ m resolution in three dimensions with a maximum displacement of 6 inches along each axis. Gases are supplied to the burner through a stainless steel gas line which enters the chamber through the bottom of the containment vessel. The flow rates of the reactant gases are regulated by Vacuum General DynaMass mass flow controllers. A nitrogen shroud gas is also admitted to the chamber through a bottom access port and is regulated through a manual valve.

Table 1. Flame Conditions Employed in this Study

Flame	Flow Rate in slpm			
	CH ₄	N ₂ O	NO	O ₂
I	0.250	-	0.360	0.500
II	0.250	1.000	-	-

The flow rates of the gases used in this study are shown in Table 1. The vertical distance from the burner where the measurements were taken was chosen to simplify the referencing of the relative profiles to the absolute concentrations. The relative profiles obtained using LIF were examined and the distance from the burner surface to the location of the maximum relative signal was identified. This was the location chosen for the focal volume in the absorption experiment. This allowed the relative profiles to be scaled easily between zero and the maximum signal. The distances from the burner surface used for the various radicals examined in this experiment are shown in Table 2. Also, all the experiments were conducted at 63 Torr to match the conditions of the LIF studies.

Table 2. Distance From Burner Surface

Radical	Distance from Burner Surface (mm)	
	Flame I	Flame II
OH	6.0	6.0
CN	3.0	3.0
NH	2.7	-

Illumination Source, Optics, and Electronics

The UV light source used was a continuous mode super-quiet xenon lamp with a 150 W power supply, both manufactured by Hamamatsu Corporation. This combination

provides continuous UV light with an intensity variation of <1% at a single wavelength (0.2 cm^{-1} bandwidth). The arc lamp was mounted inside a lamp housing also manufactured by Hamamatsu.

The point source xenon arc lamp emission was collimated using a precision-ground quartz optical lens. All lenses used in this experiment are precision-ground quartz and have a focal length of 25 cm. The lenses were secured using adjustable optical mounts to aid in the alignment procedure. The mounts were secured to the working surface either with magnetic mounts or mounting screws. The continuous wave light source was chopped using a multi-speed chopper from EG&G PARC. The chopped light was focused into the flame zone and re-collimated after exiting the chamber using a pair of lenses. The image was turned horizontally using a mirrored image rotator. The image was finally focused onto the slit of the spectrometer.

The spectrometer used in this experiment is a Spex 1702 3/4 meter with a 2400 gr/mm grating controlled by a CD2 CompuDrive. The spectrometer incorporates an RCA 31034A Photomultiplier tube (PMT). The PMT is powered by an EG&G Ortec 556 high-voltage power supply. The PMT output along with the output from the chopper were directed to a SR510 Lock-In Amplifier manufactured by Stanford Research Systems. The signal output from the lock-in amplifier was passed to a MacADIOS A/D card controlled by an Apple Macintosh IIx computer. The data collection rate was set by a trigger passed to the A/D board from a Stanford Research DG-535 digital delay generator. Data were collected and displayed in real time using data collection software written in-house and stored on disk for future analysis.

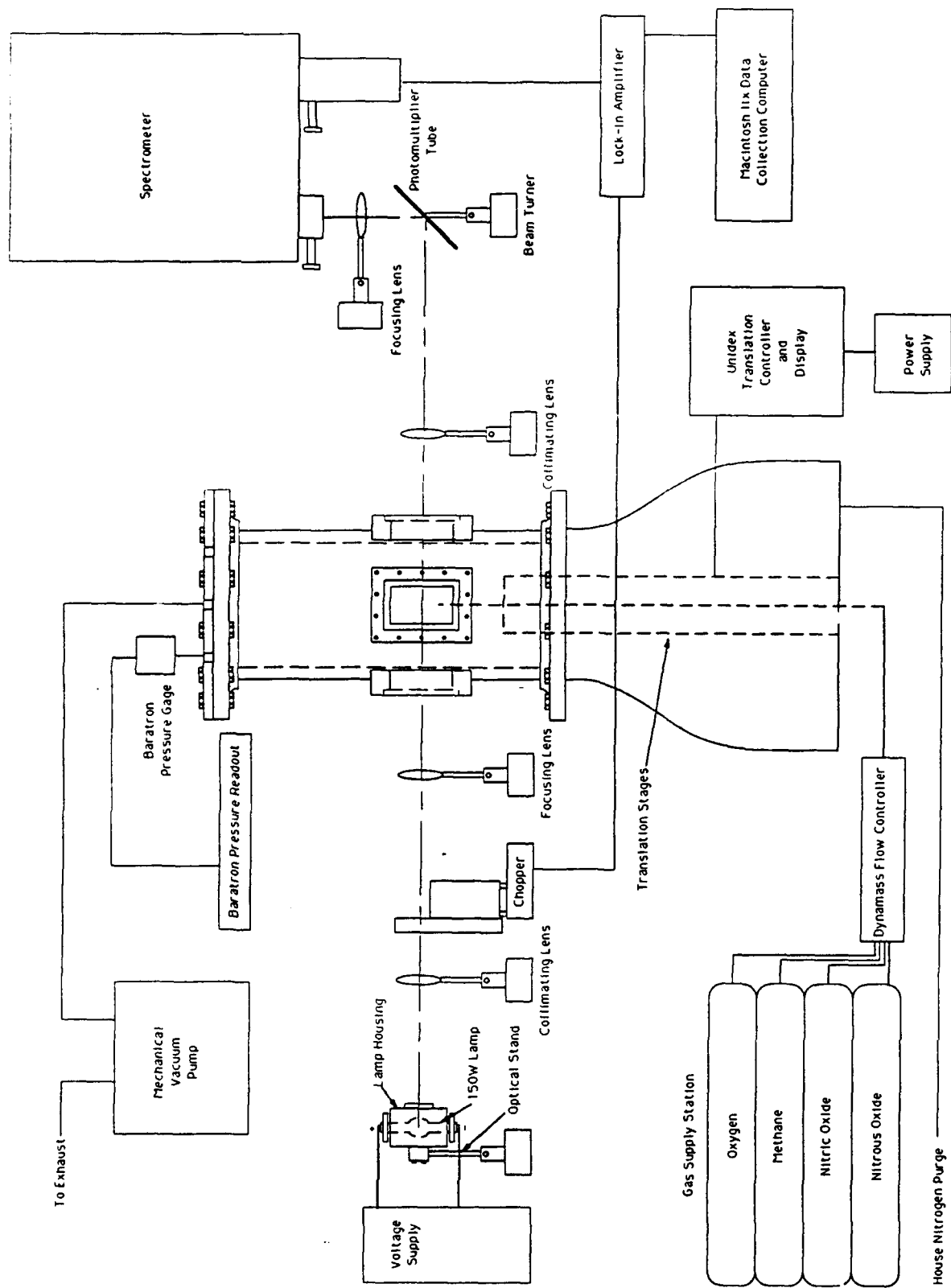


Figure 1. Schematic of Experimental Apparatus for Absorption Studies

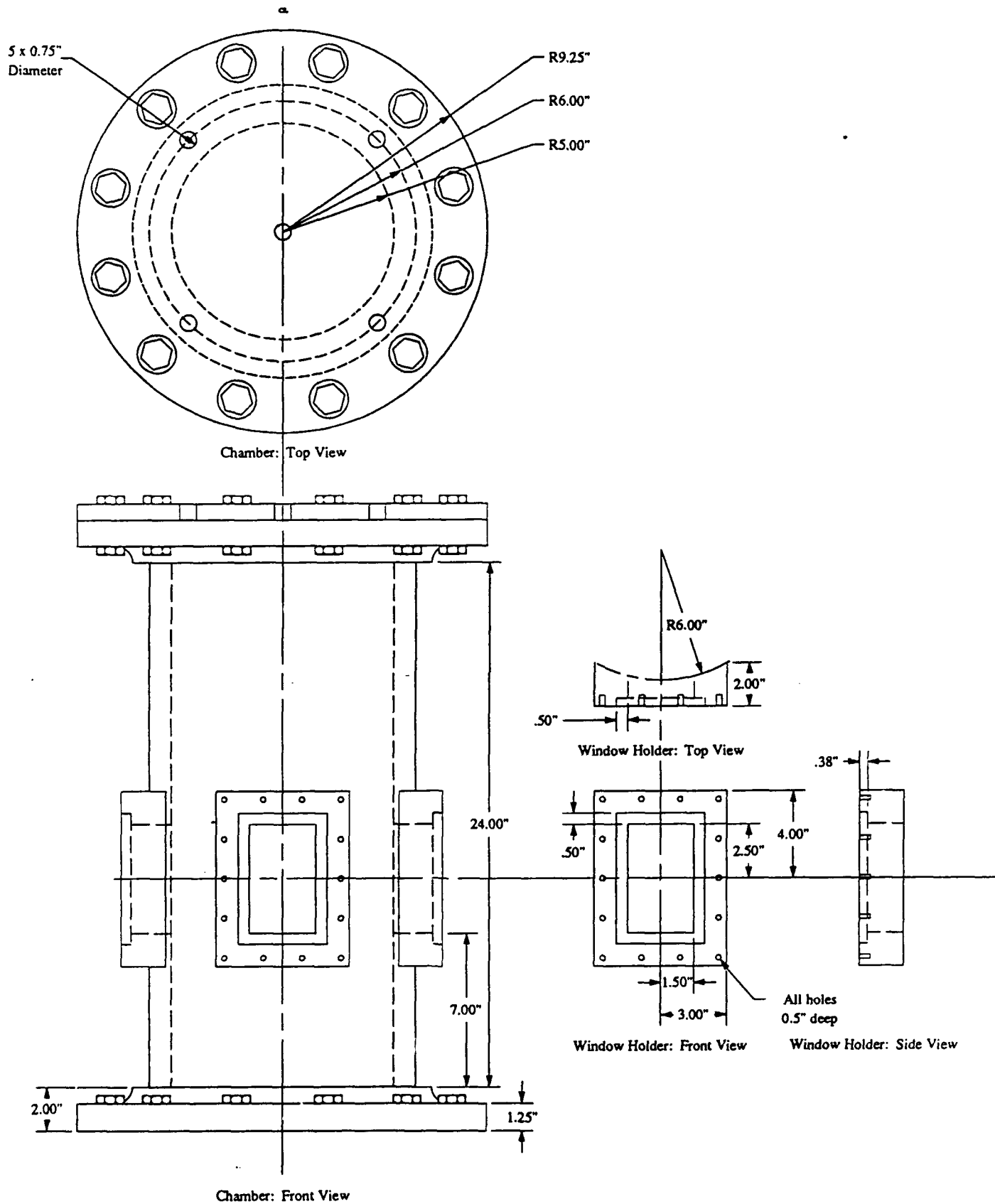


Figure 2. Burner Chamber

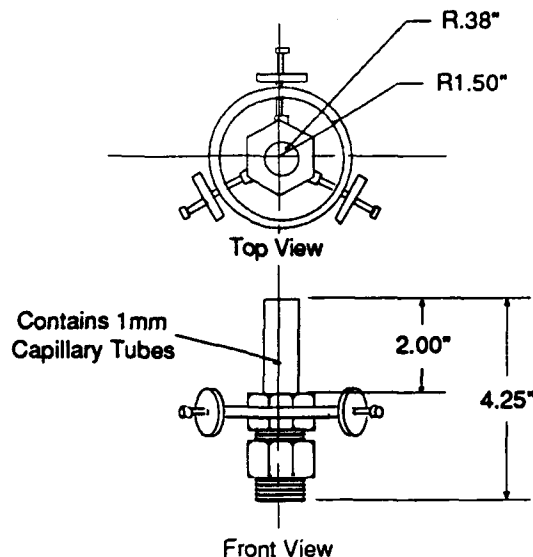


Figure 3. Flat Flame Burner

Determination of Photomultiplier Tube Saturation Level

When performing this experiment, care must be taken to insure that the photomultiplier tube is not saturated. To insure that the PMT was indeed unsaturated, a neutral density filter was used to attenuate the incident light entering the spectrometer. The resulting drop in measured intensity was noted. If the measured absorption due to the filter was found to be less than the optical density of the filter, saturation of the PMT was assumed and the spectrometer slits were adjusted to eliminate this effect.

Determination of Burner Surface Position

The burner surface was defined as the vertical location where the output of the PMT is equal to the average of the maximum and minimum signal output obtainable at a specific wavelength. To determine this position, the experimental systems were first started but the burner was not ignited. The burner was positioned using the translation controller so that through visual inspection, the light beam was noted to be well below the burner. At this time, the burner was positioned through visual inspection so that the beam intersected the horizontal center of the burner side. This position represented total blockage of the light beam. This minimum PMT output was noted and the burner was lower until the beam was completely exposed and the signal leveled off to a maximum. The average of the minimum and maximum was calculated and the burner was raised until this value was obtained. This position was defined to be the location where 1/2 of the beam is blocked by the burner surface. This method has proven to be a reliable method for burner surface location through visual inspection of the beam location on the burner. The Unidex translation control unit was reset with this position representing the origin (0,0,0) and all further burner positions were measured from this location.

Method for Relating Absorption Profiles to Absolute Concentrations

Integrated absorptions were measured by scans recorded across single rotational lines. The absorption profiles for a single absorption line of the spectra were plotted

relative transmission vs. relative frequency (cm^{-1}) and integrated using a Macintosh graphics application (Igor from WaveMetrics) to obtain the area under the absorption curve (in units of cm^{-1}). A typical absorption profile for the $Q_1(6)$ line of the OH radical is shown in Fig. 4.

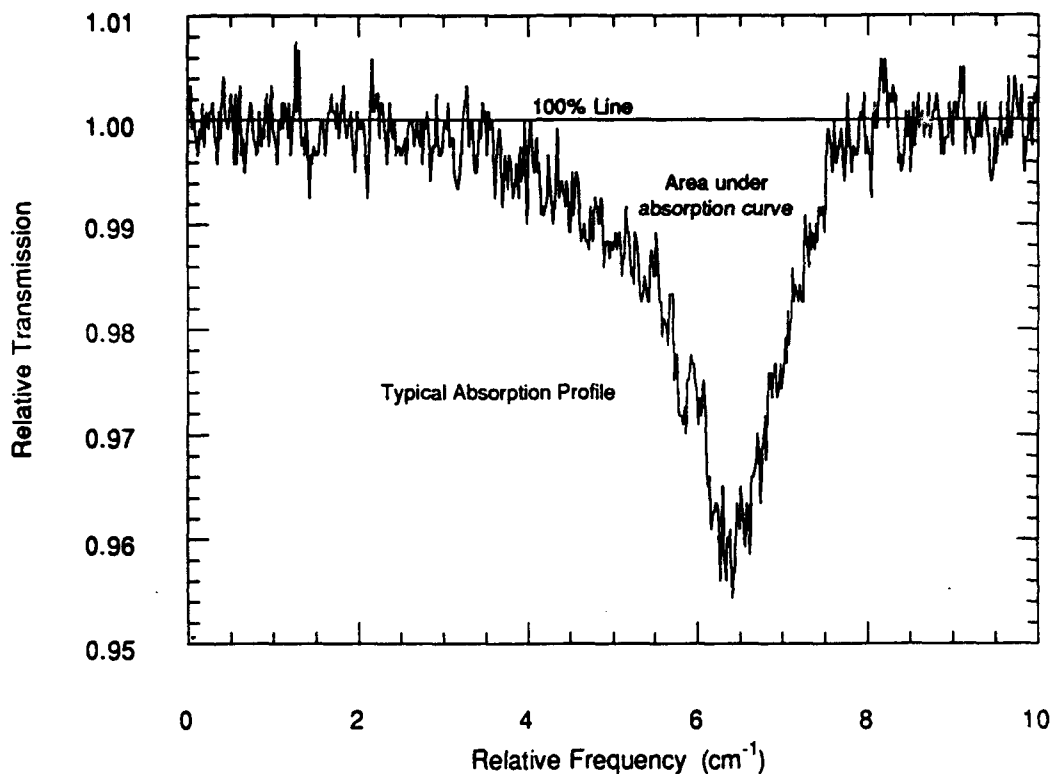


Figure 4. Typical Absorption Profile

This area, the integrated absorption, $\int W_{\omega} d\omega$, was related to the radical concentration by the following method discussed in detail by Lucht et al. [Ref. 1].

As radiation passes through the flame, the reduction in incident intensity I_{ω} is related to the path length, l , by Beer's law:

$$T_{\omega} = \frac{I_{\omega}(l)}{I_{\omega}(0)} = e^{-k_{\omega}l} \quad (1)$$

where T_{ω} is the spectral transmission, $I_{\omega}(0)$ and $I_{\omega}(l)$ are the spectral intensities before the flame and after passing through a path length l , respectively, and k_{ω} is the spectral absorption coefficient. The spectral absorptivity A_{ω} is obtained by rearranging equation 1 to yield:

$$A_{\omega} = 1 - T_{\omega} = \frac{I_{\omega}(0) - I_{\omega}(l)}{I_{\omega}(0)} \quad (2)$$

The spectral absorption coefficient, k_{ω} is defined by

$$k_{\omega} = K_{ji} Y(\omega) \quad (3)$$

where K_{ji} is the line strength for transition from level j to level i and is independent of ω , and $Y(\omega)$ is the line profile, which accounts for the line broadening. Combining equations 1-3 gives the following equation for the spectral absorptivity:

$$A_{\omega} = 1 - \exp[-K_{ji} Y(\omega) l] \quad (4)$$

When including simultaneous Doppler, collisional, and natural broadening effects, the line profile $Y(\omega)$ becomes the so-called Voigt profile:

$$Y(\omega) = \frac{2\sqrt{\ln 2}}{\sqrt{\pi}\Delta\omega_D} V(\xi, a) \quad (5)$$

where $\Delta\omega_D$ is the Doppler half width and the Voigt function $V(\xi, a)$ is defined as:

$$V(\xi, a) = \frac{a}{\pi} \int_{-\infty}^{\infty} \frac{\exp(-y^2) dy}{a^2 + (\xi - y)^2} \quad (6)$$

The integrated absorption, or equivalent width $W_{J''J'}$ is defined by equation 7:

$$W_{J''J'} = \int_{\omega_1^*}^{\omega_2^*} A_{\omega} d\omega \quad (7)$$

where ω_1^* and ω_2^* are the limits of the spectral line.

Combining equations 4 and 7 and substituting $K_{J''J'}$ for K_{ji} where the j and i levels are the J'' and J' rotational levels, respectively, we obtain:

$$W_{J''J'} = \int_{\omega_1^*}^{\omega_2^*} \{1 - \exp[-K_{J''J'} Y(\omega) l]\} d\omega \quad (8)$$

Using equation 5 we then get:

$$W_{j''j'} = \int_{\omega_1^*}^{\omega_2^*} \left(1 - \exp \left[-K_{j''j'} \frac{2\sqrt{\ln 2}}{\Delta\omega_D \sqrt{\pi}} V(\xi, a) \right] \right) d\omega \quad (9)$$

Using the identity in equation 10, equation 9 can be put in terms of one variable, ξ :

$$d\omega = \frac{\Delta\omega_D}{2\sqrt{\ln 2}} d\xi \quad (10)$$

$$W_{j''j'} = \frac{\Delta\omega_D}{\sqrt{\ln 2}} \int_0^{\xi_1^*} \left(1 - \exp \left[-K_{j''j'} \frac{2\sqrt{\ln 2}}{\Delta\omega_D \sqrt{\pi}} V(\xi, a) \right] \right) d\xi \quad (11)$$

Notice that because the Voigt profile is symmetric about $\xi=0$, integration was performed over one-half of the line and the result multiplied by two.

As it turns out, this expression (Equation 11) cannot be analytically integrated, therefore numerical methods must be employed. A step-wise integration routine was used to evaluate the expression. The first difficulty in integrating this equation is the evaluation of the Voigt profile. A technique for the evaluation of this integral was published by Armstrong [Ref. 3], and it was this method which was used. The Voigt profile was evaluated for each stepwise position in this integration routine. The Voigt profile is graphed for several values of a in Fig. 5. The numerical value of the Voigt function was then substituted into the equation and the "outer" function was numerically integrated using an extended trapezoidal version of Simpson's rule [Ref. 4]. Data sets were calculated for varying values of the broadening parameter, a , and for different line strengths $K_{j''j'}$

(Appendix B). When the resulting data was plotted $\ln \left(W_{j''j'} \frac{\sqrt{\ln 2}}{\Delta\omega_D} \right)$ versus

$\ln \left(K_{j''j'} \left[1 - \frac{2\sqrt{\ln 2}}{\Delta\omega_D \sqrt{\pi}} \right] \right)$ for a given value of a , the so-called "curves of growth" were

generated as shown in Fig. 6. A listing of the code used to produce this data is provided in Appendix A. The program was written using Think C 4.0 from Symantec running on an Apple Macintosh IIx personal computer.

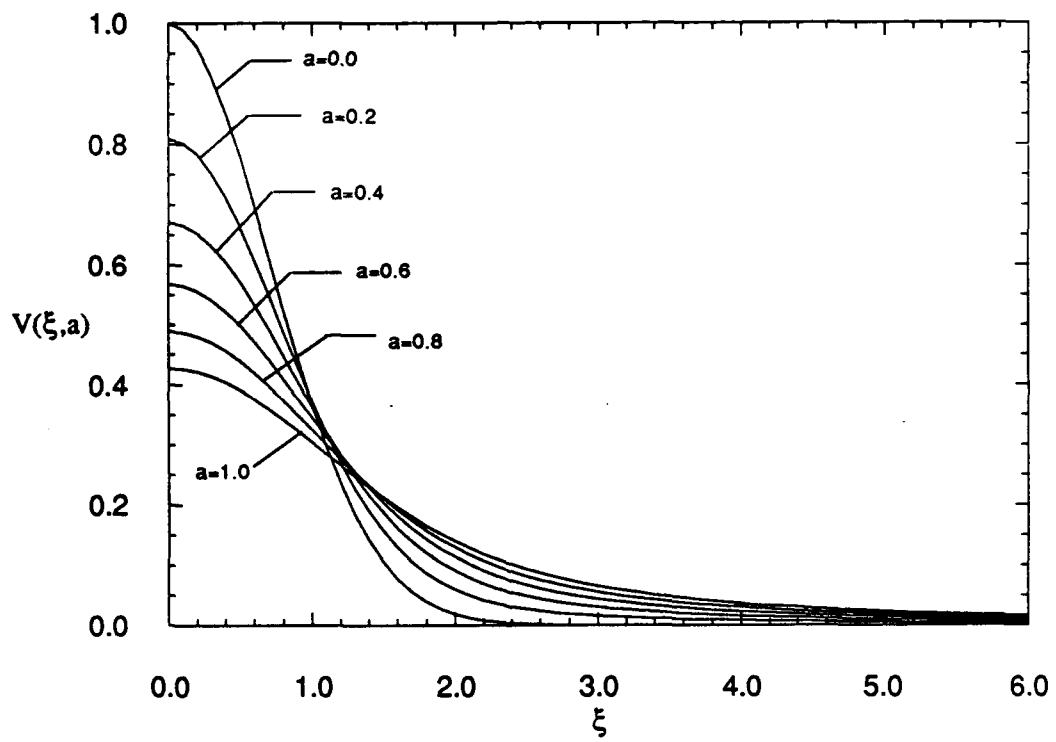


Figure 5. Voigt Profiles for Various Values of the Broadening Parameter

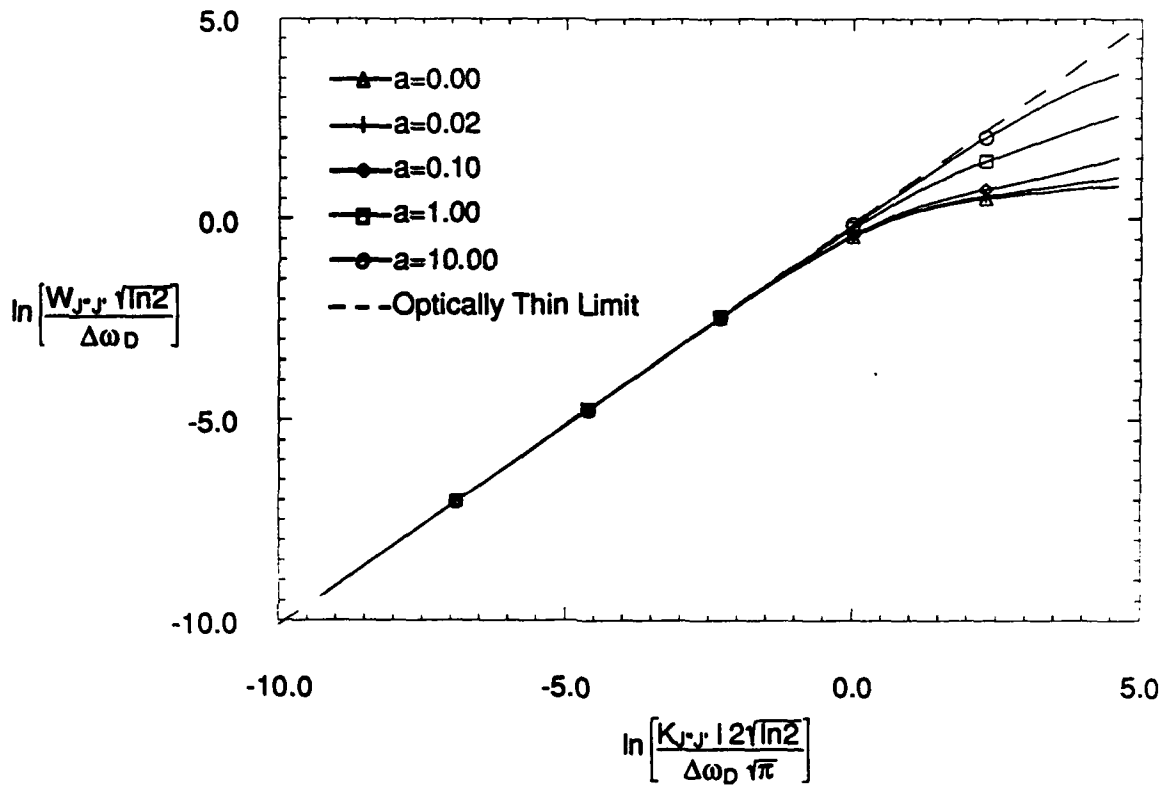


Figure 6. Curves of Growth Plots for Various Values of the Broadening Parameter

These so-called "curves of growth" provide a way of correcting for absorptions obtained under non-optically thin conditions. The optically thin limit is shown by the dashed line in Fig. 6. When the absorbing medium is optically thin (i.e., the gas is weakly absorbing) $K_{J''J'} l \ll 1$, and equation 8 can be rewritten using the relation $e^x = 1 + x$,

$$W_{J''J'} = \int_{\omega_1^*}^{\omega_2^*} [K_{J''J'} Y(\omega) l] d\omega \quad (12)$$

Using the fact that the line profile is normalized,

$$\int_{\omega_1^*}^{\omega_2^*} Y(\omega) d\omega = 1 \quad (13)$$

Integration of equation 12 yields,

$$W_{J''J'} = K_{J''J'} l \quad (14)$$

Thus, in the optically thin limit the integrated absorption is directly proportional to both the path length and the number density of the absorber. Figure 6 demonstrates that deviation from the optically thin limit occurs for $\left(W_{J''J'} \frac{\sqrt{\ln 2}}{\Delta\omega_D}\right) > 1$. For a typical doppler width in a flame of 0.2 cm^{-1} and a typical measured value of the half-width of the integrated absorption of 2 cm^{-1} , this yields a peak absorption of 24%. Thus, optically thin limit conditions hold for peak absorptions of <20%. As will be seen later in this study, all absorptions measured here were <5% and thus are operating very close to the optically thin limit. The above "curves of growth" correction is very small in these studies.

Once the relationship between actual integrated absorption $W_{J''J'}$ and line strength $K_{J''J'}$ is determined, the number density at the particular line can be determined from equation 15.

$$N_{J''} = \frac{m_e c^2}{\pi e^2} \frac{K_{J''J'}}{f_{v''v'}} \frac{2J''+1}{S_{J''J'} T_{J''J'}} \quad (15)$$

where $\frac{m_e c^2}{\pi e^2} = 1.133 \times 10^{12} \text{ cm}^{-1}$, $f_{v''v'}$ is the band oscillator strength for transition from lower vibrational level v'' to upper vibrational level v' , $S_{J''J'}$ is the rotational line strength and $T_{J''J'}$ is a correction factor used in calculating band oscillator strengths to account for the increased inter-nuclear separation at higher rotational quantum numbers. Equation 16 is used to relate the number density at a particular rotational level, $N_{J''}$, obtained from equation 15, to the overall number density, N .

$$N = N_{J''} \frac{Q_e Q_v Q_r}{2J''+1} \exp\left(\frac{hc}{kT} [T_e(n) + G(v) + F(J'')]\right) \quad (16)$$

where $T_e(n)$ is the electronic term energy, $G(v)$ is the vibrational term energy for level v , and $F(J'')$ is the rotational term energy for level J'' . Q_e , Q_v , and Q_r are the electronic, vibrational, and rotational partition functions and are given by equations 17, 18, and 19, respectively.

$$Q_e = \sum (2S+1) \phi \exp\left[\frac{-hcT_e(n)}{kT}\right] \quad (17)$$

where S is the spin quantum number, ϕ equals 2 when $\Lambda \neq 0$, and 1 when $\Lambda = 0$, and T is the temperature at the point of interest in the flame.

$$Q_v = \sum \exp\left[\frac{-hcG(v)}{kT}\right] \quad (18)$$

$$Q_r = \frac{kT}{hcB_v} \quad (19)$$

B_v is the rotational constant. Substituting the values from equation 17-19 into equation 16 yields the desired result, the absolute number of molecules of the free radical at the point of interest in the flame. A sample calculation for the OH radical in the $\text{CH}_4/\text{N}_2\text{O}$ flame can be found in Appendix C.

Results

Emission Spectroscopy

The criteria which were used for choosing a rotational line with which to perform absorption measurements were as follows: the line must probe the ground vibrational state of the molecule, the line must be isolated and not blended with any other lines, and it must be one of the stronger lines in order to improve the signal-to-noise ratio. Emission spectra for the three radicals were taken to identify candidate spectral lines. The emission spectra taken for OH, CN, and NH are shown in Figs. 7, 8, and 9, respectively. The emission work was performed in the same chamber as the absorption experiments.

OH Emission

The line used in the OH measurements was the $Q_1(6)$ transition of the 0,0 vibrational band of the $A^2\Sigma^+ - X^2\Pi$ electronic transition which is located at 308.73 nm [Ref. 5]. A portion of the spectrum obtained in a 58 Torr CH_4/O_2 flame with an equivalence ratio of 1.25 over the wavelength range 306 to 310 nm is shown in Fig. 7.

CN Emission

The line used in the CN measurements was the unresolved $R(15)$ doublet of the 0,0 vibrational band of the $B^2\Sigma^- - X^2\Sigma$ electronic transition which is located at 386.34 nm [Ref. 6]. At the resolution employed ($\approx 0.3 \text{ cm}^{-1}$) this doublet could not be resolved. The spectrum for CN obtained in the N_2O flame (Flame II) between 385.5 and 388.5 nm is shown in Fig. 8.

NH Emission

The line used in the NH measurements was the $R_2(8)$ transition of the 0,0 vibrational band of the $A^3\Pi - X^3\Sigma^-$ electronic transition which is located at 332.69 nm [Ref. 7]. The spectrum for NH obtained in the N_2O flame (Flame II) between 332 and 338 nm is shown in Fig. 9. The $R_2(8)$ line is the middle line of a well resolved triplet.

Absorption Spectroscopy

Absorption scans were performed over the applicable spectral transitions in the flames studied. The very small absorptions found in these flames necessitated that the authors choose a careful balance of scan rate and detector resolution. Slow scan rates allow greater signal averaging and thus a better signal-to-noise level. Scans performed too slowly may allow changes in the flame to occur. Low resolution scans permit adjacent spectral lines to be readily resolved, but noise increases significantly using narrow slit widths. Thus a balance of these parameters had to be chosen to maximize signal levels, minimize noise and permit reasonably short scans. Typical scan times chosen were ≈ 20 minutes for scans of 6 to 18 cm^{-1} .

OH Absorption

Typical absorption profiles for the $Q_1(6)$ transition in the two flames are shown in Fig. 10. The absorption profiles were graphically integrated using a data analysis/graphics application called Igor (WaveMetrics). Three trials were individually integrated for each

flame and the resulting areas were then averaged. The average integrated areas for both flames are shown in Table 3. The standard deviation of these three trials was ± 0.002 .

CN Absorption

Typical absorption profiles for the R(15) doublet transition in the two flames are shown in Fig. 11. Three absorption scans were performed for each concentration measurement. Unlike the trials for OH, the individual absorption profiles were first themselves averaged, and a Gaussian curve fit was performed. The average integrated area of the Gaussian fit was then determined. The average integrated areas for the two flames are shown in Table 3.

NH Absorption

Typical absorption profiles for the triplet containing the R₂(8) transition in the N₂O flame is shown in Fig. 12 along with an isolation on the R₂(8) line itself. The NH absorption profiles were treated much the same as the CN profiles. Three individual absorption scans in the N₂O flame were first averaged, and a Gaussian curve fit was applied. An average integrated area was then determined from this curve fit. The average integrated area is shown in Table 3. An absorption signal could not be detected in the NO flame, therefore only an upper limit on the NH concentration could be estimated.

Table 3. Integrated Areas for OH, CN, and NH Absorption Profiles in CH₄/N₂O and CH₄/NO/O₂ Flames at 63 Torr

Species	Average Integrated Areas	
	CH ₄ /N ₂ O Flame	CH ₄ /NO/O ₂ Flame
OH	0.0842 cm ⁻¹	0.0761 cm ⁻¹
CN	0.00983 cm ⁻¹	0.00573 cm ⁻¹
NH	0.0104 cm ⁻¹	-

The absolute concentrations determined for the three radicals in both flames is shown in Table 4. No absorption signal could be detected for NH in the CH₄/N₂O flame and therefore the value shown in the table is an estimated upper limit, i.e., an estimate of the maximum concentration of NH that could be in the flame and still have the absorption profile be undetectable.

Table 4. Absolute Concentrations of OH, CN, and NH in CH₄/N₂O and CH₄/NO/O₂ Flames at 63 Torr

Species	Transition	Peak Mole Fraction	
		CH ₄ /N ₂ O Flame	CH ₄ /NO/O ₂ Flame
OH	Q ₁ (6), 0-0, 308.73 nm	(1.2±0.4) × 10 ⁻²	(9±4) × 10 ⁻³
CN	R(15) doublet, 0-0, 386.34 nm	(5.9±2.4) × 10 ⁻⁵	(2.9±1.2) × 10 ⁻⁵
NH	R ₂ (8), 0-0, 332.69 nm	(4.8±2.0) × 10 ⁻⁴	<1 × 10 ⁻⁴

Conclusions

Absorption spectroscopy techniques were used for measurement of absolute concentrations of free radical species in premixed, laminar, flat-flames of $\text{CH}_4/\text{N}_2\text{O}$ and $\text{CH}_4/\text{NO}/\text{O}_2$. Absolute concentration measurements were performed for the species OH, CN, and NH in 63 Torr flames. These absolute concentration measurements were used to calibrate relative concentration profiles taken in previous experiments using laser-induced fluorescence (LIF) spectroscopy. Significant absorptions of these species could be obtained even in the very short path length flames studied. These measurements permitted the experimental LIF measurements to be directly compared to the species concentration profiles predicted by the CHEMKIN/PREMIX flame modeling code.

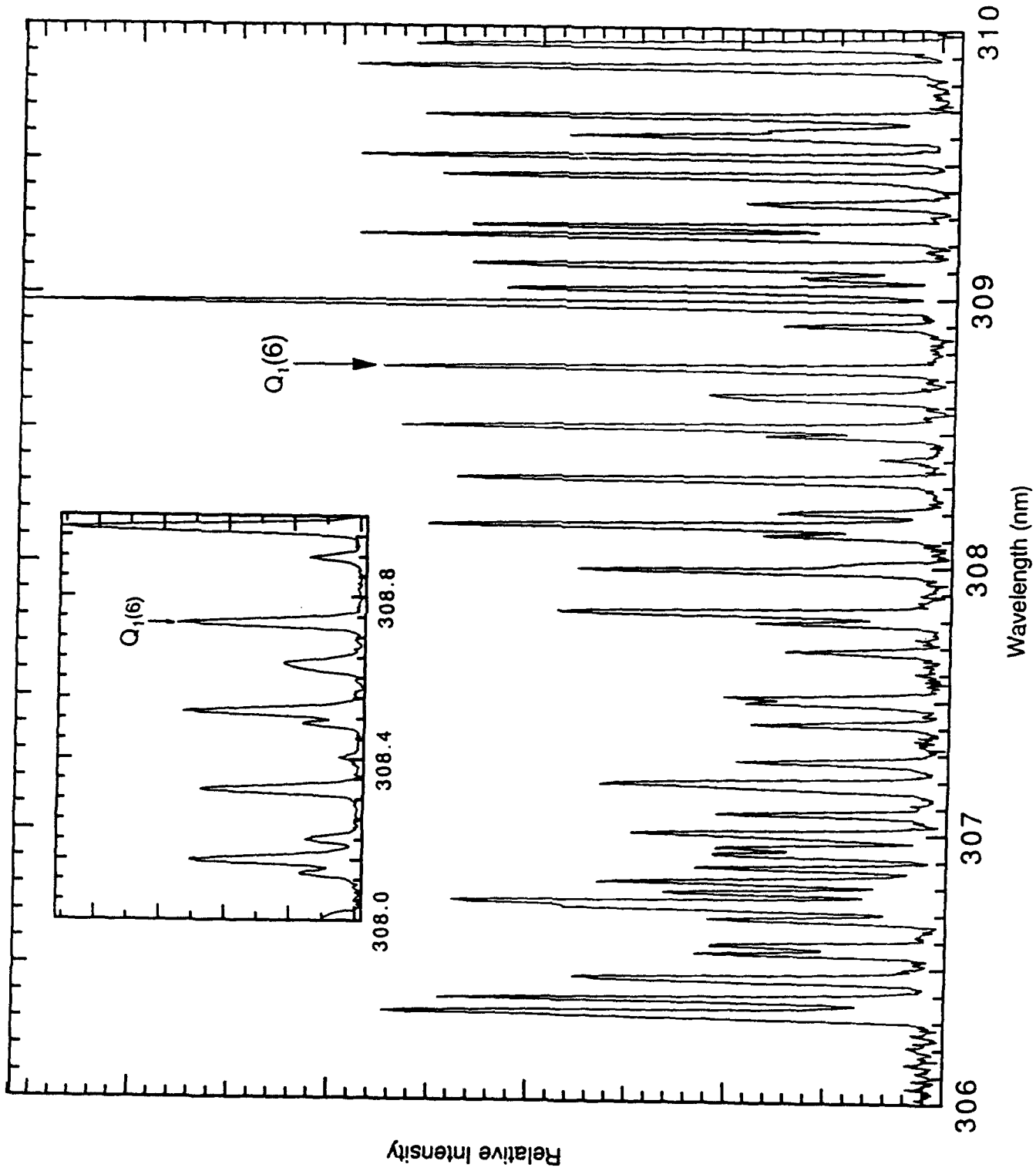


Figure 7. Emission Spectrum for the OH radical from 306 to 310 nm.

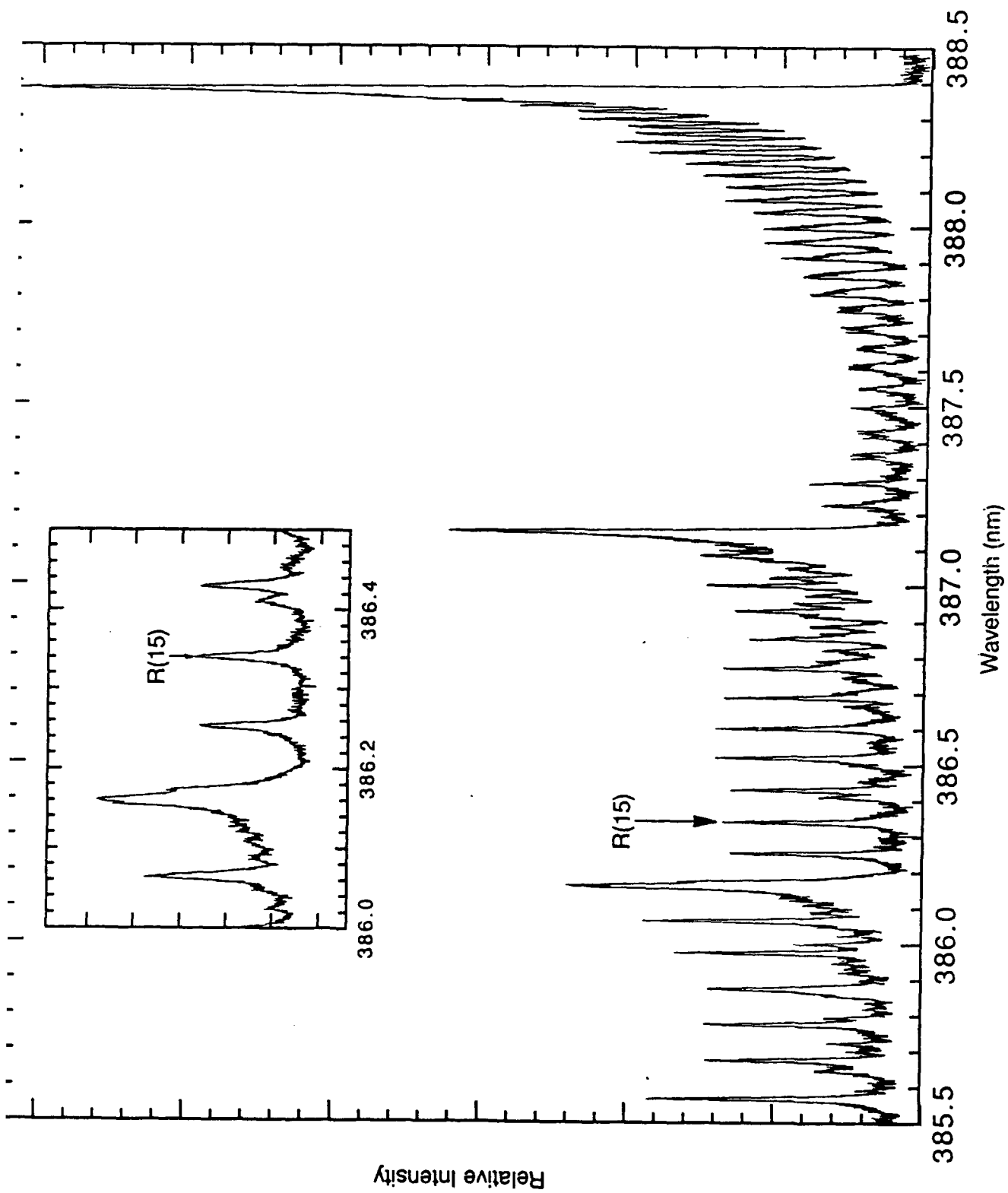


Figure 8. Emission Spectrum for the CN radical from 385.5 to 388.5 nm.

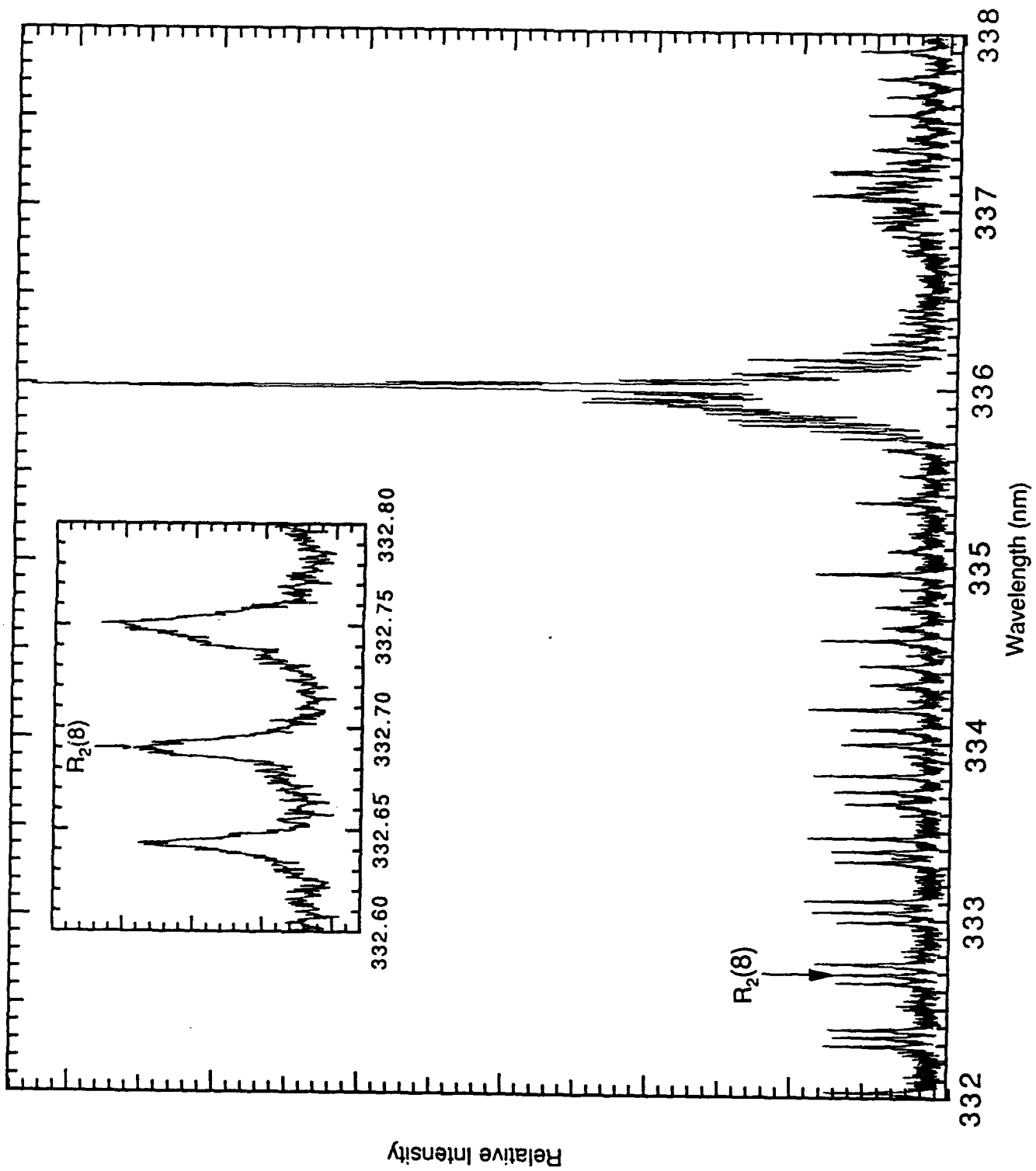


Figure 9. Emission Spectrum for the NH radical from 332 to 338 nm.

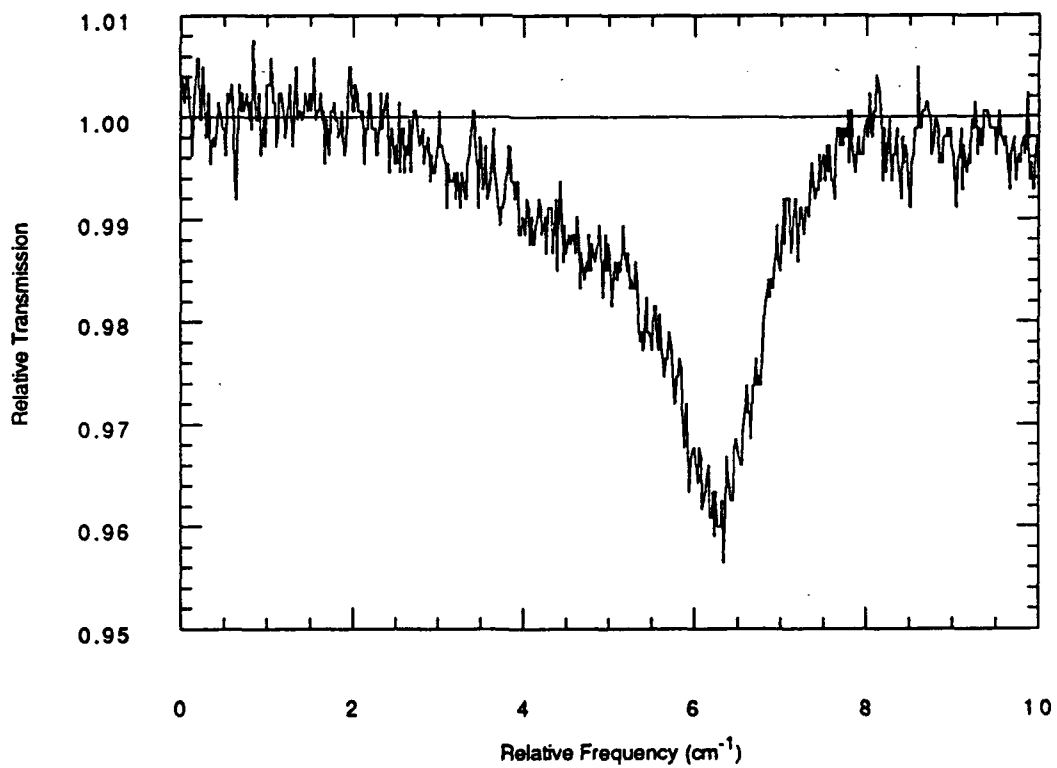
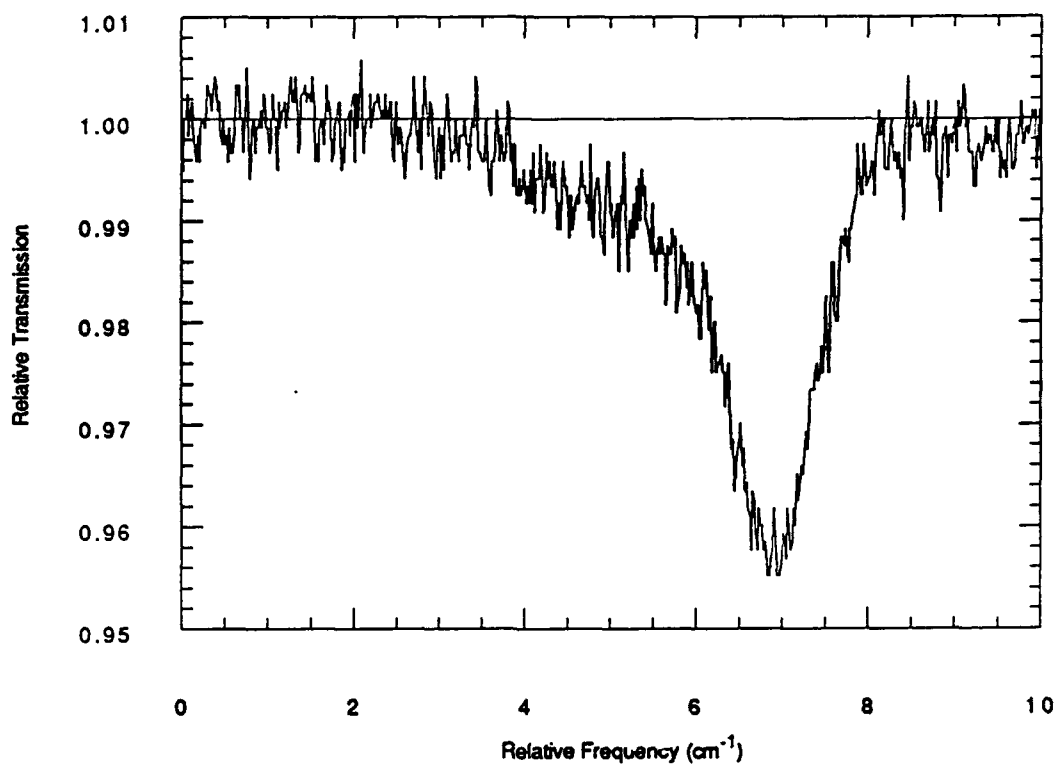


Figure 10. Absorption Profiles for the Q₁(6) transition of OH.
Top: CH₄/N₂O flame; bottom: CH₄/NO/O₂ flame.

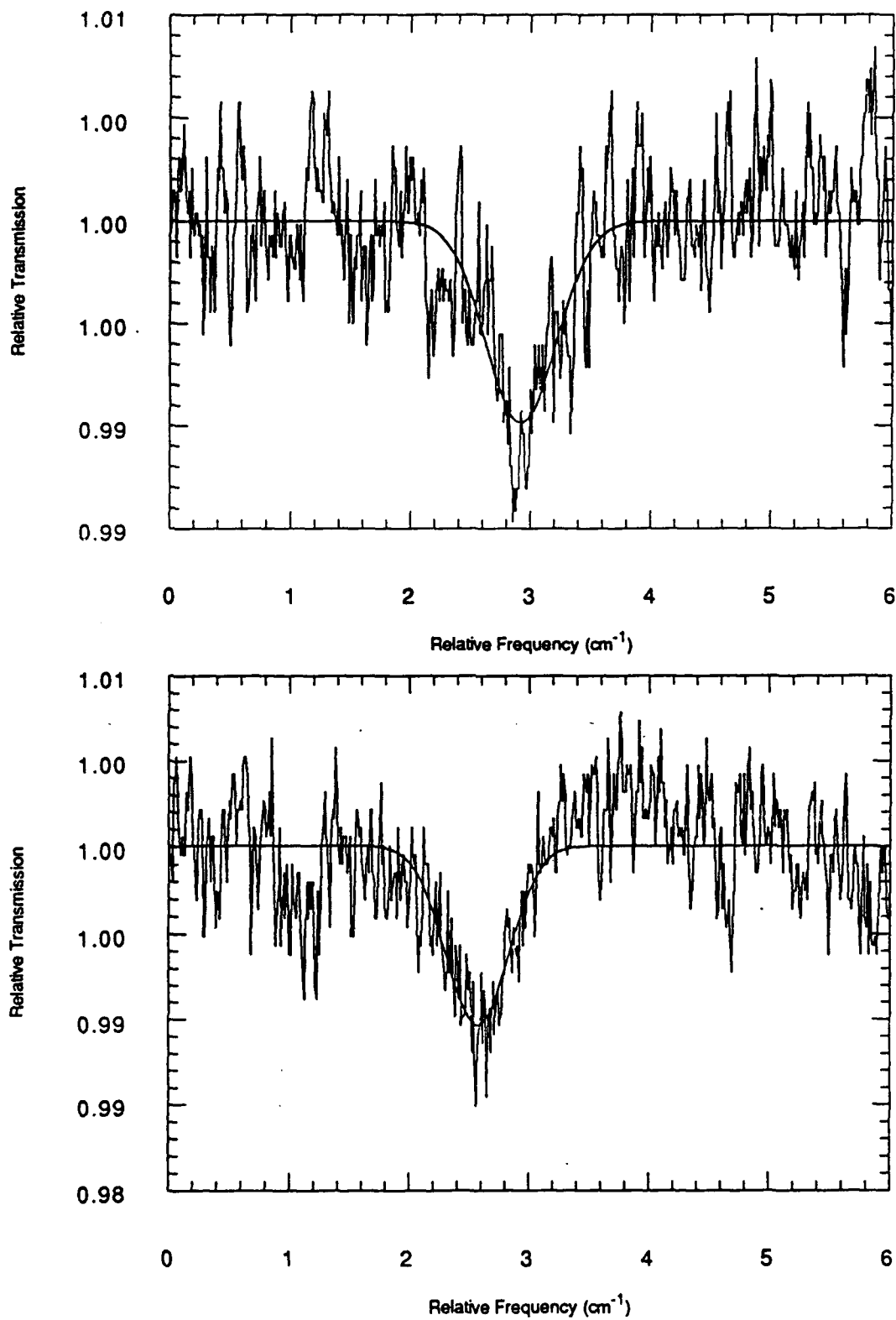


Figure 11. Absorption Profiles for the unresolved R(15) doublet of CN. Top: CH₄/N₂O flame; bottom: CH₄/NO/O₂ flame.

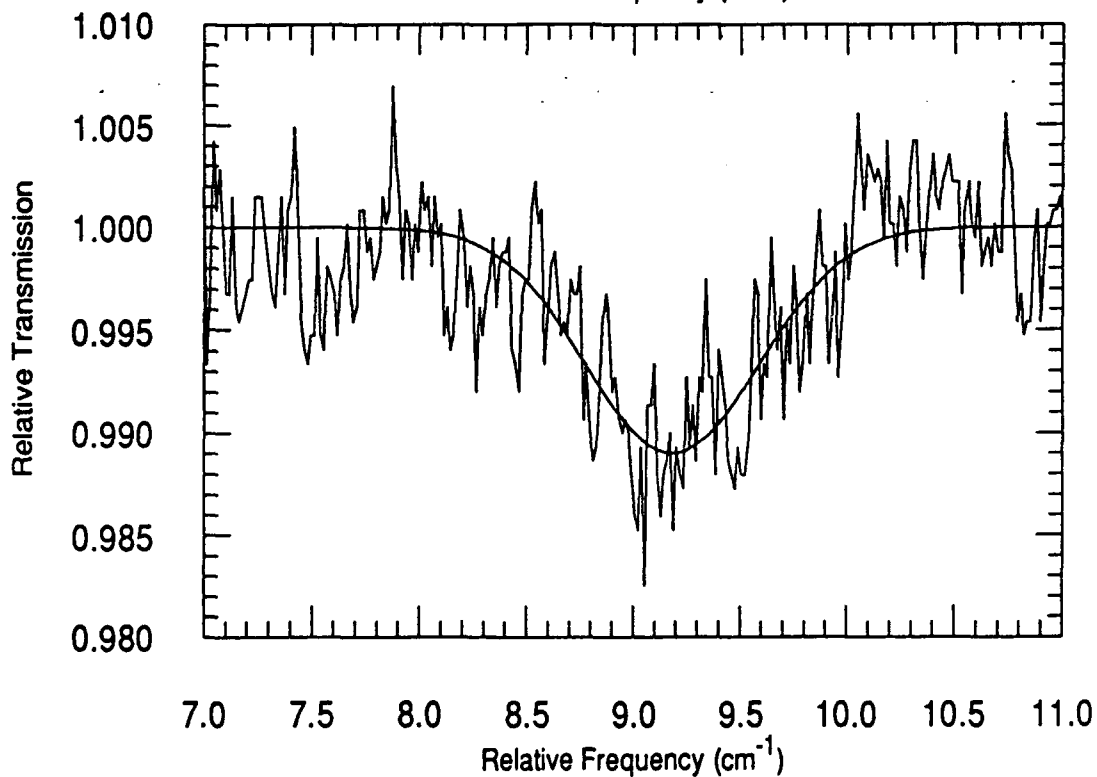
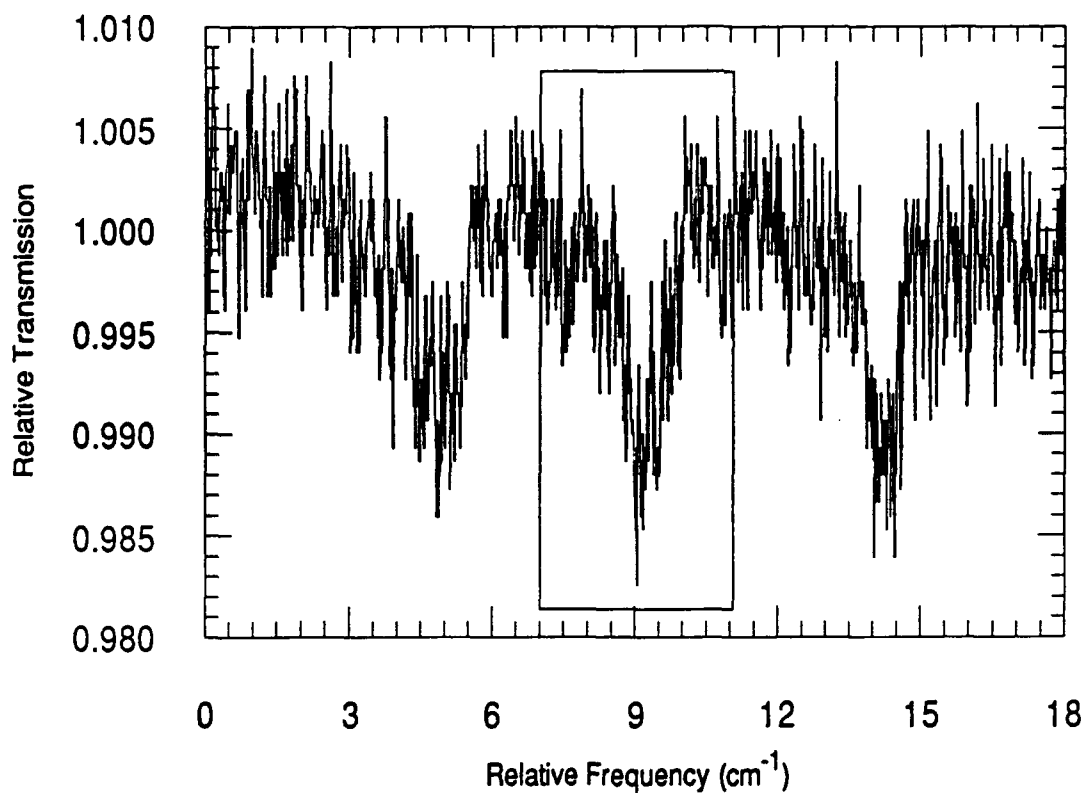


Figure 12. Absorption Profiles for the R(8) transitions of NH.
 Top: R(8) triplet in the CH₄/N₂O flame; bottom: R₂(8) transition.

References

1. Lucht, R.P., Peterson, R.C., and Laurendeau, N.M., "Fundamentals of Absorption Spectroscopy for Selected Diatomic Flame Radicals," Purdue Report PURDU-CL-78-06, 1978.
2. Zabarnick, S., "A Comparison of CH₄/NO/O₂ and CH₄/N₂O Flames by LIF Diagnostics and Chemical Kinetic Modeling," Combustion Sci. Tech., submitted for publication.
3. Armstrong, B.H., "Spectrum Line Profiles: The Voigt Function," Journal of Quantitative Spectroscopy and Radiative Transfer, Vol. 7, pp. 61-88, 1967.
4. Press, W.H., Flannery, B.P., Teukolsky, S.A., and Vetterling, W.T., Numerical Recipes in C: The Art of Scientific Computing, Cambridge University Press, New York, 1989.
5. Dieke, G.H., and Crosswhite, H.M., "The Ultraviolet Bands of OH - Fundamental Data," Journal of Quantitative Spectroscopy and Radiative Transfer, Vol. 2, pp. 97-199, 1962.
6. Jevons, W., "The More Refrangible Band System of Cyanogen as Developed in Active Nitrogen," Proceedings of the Royal Society, Series A, Vol. 112, pp. 407-44, 1926.
7. Dixon, R.N., "The 0-0 and 1-0 Bands of the A(³Π_j)-X(³Σ⁻) Systems of NH," Canadian Journal of Physics, Vol. 37, pp. 1171-1186, 1959.

Appendix A. Listing of Curves of Growth Integration Routine

The following code was written in Think C Version 4.0 on a Macintosh IIx personal computer. It has been left in ANSI C format to allow for greater portability. The standard integration was performed using a trapezoidal variation on Simpson's rule found in Numerical Recipes in C [Ref. 4]. The Voigt function was integrated using a routine published by Armstrong [Ref. 3] which was converted from FORTRAN to C.

The program generates a specific column of data such as that found in Appendix B. The particular value of the broadening parameter is entered as parameter2, which in the sample code is equal to 2. The range and step size of the values of the x-axis of Fig. 6,

$\ln \left(\frac{K_J \cdot J \cdot 1 \cdot 2 \cdot \sqrt{\ln 2}}{\Delta \omega_D \sqrt{\pi}} \right)$ are given by the variables MINIMUMTABLE,

MAXIMUMTABLE, and TABLESTEP. The initial value is set in MINIMUMTABLE, the final value is set in MAXIMUMTABLE, and the incremental step size between the two values is set in TABLESTEP. The program outputs a set of two column data to the screen.

/*.....*/

Curves of Growth Integration Routine
Numerical Solver
David A. Alspach
Astronautics Laboratory (AFSC/LSCC)
and
Steven Zabarnick
University of Dayton Research Institute

/*.....*/

/*.....*/

Section: includes, defines, prototyping, and global
initialization
Type: initialization section
Date: 30 October 1990
Description: includes standard C library's, sets up define and
global variables, and prototypes all function to be used
in the program.

/*.....*/

#include <math.h>
#include <stdio.h>

#define EPS 1.0e-5
#define JMAX 20
#define FUNC(x) ((*func)(x))

#define MINIMUMTABLE 0.0001 /* First Kjj term in table */
#define MAXIMUMTABLE 0.0010 /* Final Kjj term in table */
#define TABLESTEP 0.0001 /* Kjj term increment steps*/

float func(float x);
float qsimp(float (*func)(), float a, float b);
float trapzd(float (*func)(), float a, float b, int n);
double voigt(double x, double y);
double k1(double x, double y);
double k2(double x, double y);
double k3(double x, double y);

double w[10];
double t[10];

float parameter1; /* Variable definition for non-dimensional Kjj term*/
float parameter2; /* Variable definition for broadening parameter a */

/*.....*/

Section: main
Type: program control loop
Date: 30 October 1990
Description: sets up the stepping routines to generate curve of growth
tables.

/*.....*/

main()

(
FILE *myFile;
Point thePoint;
SFTypeList types;
SFReply reply;

float y, count;

parameter2=2.0;

```

printf("Broadening Parameter: %f\n",parameter2);
printf("Kjj term\tWjj term");
for(count=MINIMUMTABLE;count<=MAXIMUMTABLE;count=count+TABLESTEP)
{
    parameter1=count;
    y=log(qsimp(func,0,200));
    printf("%f\t%f\n",log(parameter1),y);
}
}
/*****
Section:          qsimp
Type:            function
Date:           30 October 1990
Description:     Returns the integral of the function func from a to b.
                The parameters EPS can be set to the desired fractional
                accuracy and JMAX so that 2^JMAX-1 is the maximum allowed
                number of steps. Integration is performed by Simpson's
                rule. Note: from Numerical Recipes in C.
*****/

float qsimp(func,a,b)
float a,b;
float (*func)();
{
    int j;
    float s,st,ost,os,trapzd();
    void nrerror();

    ost = os = -1.0e30;
    for (j=1;j<=JMAX;j++) {
        st=trapzd(func,a,b,j);
        s=(4.0*st-ost)/3.0;
        if (fabs(s-os) < EPS*fabs(os)) return s;
        os=s;
        ost=st;
    }
    nrerror("Too many steps in routing QSIMP");
}

/*****
Section:          trapzd
Type:            function
Date:           30 October 1990
Description:     This routine computes the n'th stage of refinement of an
                extended trapezoidal rule. func is input as a pointer to
                the function to be integrated between limits a and b, also
                input. When called with n=1, the routine returns the
                crudest estimate of the integral. Subsequent call with
                n=2,3... (in that sequential order) will improve the
                accuracy by adding 2^n-2 additional interior points.
                Note: from Numerical Recipes in C.
*****/

float trapzd(func,a,b,n)
float a,b;
float (*func)();
int n;
{
    float x,tnm,sum,dcl;
    static float s;
    static int it;
    int j;

    if (n==1) {
        it=1; /* it is the number of points to be added on the next call */
        return (s=0.5*(b-a)*(FUNC(a)+FUNC(b)));
    } else {

```

```

        tnm=it;
        del=(b-a)/tnm; /* This is the spacing of the points to be added */
        x=a+0.5*del;
        for (sum=0.0, j=1; j<=it; j++, x+=del) sum += FUNC(x);
        it *= 2;
        s=0.5*(s+(b-a)*sum/tnm); /* This replaces s by its refined value */
        return s;
    }
}

/*****
Section:          nrerror
Type:            function
Date:           30 October 1990
Description:     Numerical recipes standard error handler.
*****/

void nrerror(error_text)
char error_text[];

{
    void exit();

    fprintf(stderr, "Numerical Recipes run-time error...\n");
    fprintf(stderr, "%s\n", error_text);
    fprintf(stderr, "...now exiting to system...\n");
    exit(1);
}

/*****
Section:          func
Type:            function
Date:           30 October 1990
Description:     Section which defines function to be integrated.
*****/

float func(float x)
{
    return 1-exp(-parameter1*voigt(x, parameter2));

    /* Note:      The function contains another function 'voigt' which
                   itself is an integral function dependent on x. This
                   function is integrated using methods described by
                   Armstrong. */
}

/*****
Section:          voigt
Type:            function
Date:           30 October 1990
Description:     Function which controls the calculation of the voigt
                   profiles. This section defines the constants w and t
                   and decides which method of calculation to use depending
                   on which values of x and y are passed.
*****/

double voigt(double x, double y)
{
    double v;

    w[0]=4.62243670e-1;
    w[1]=2.86675505e-1;
    w[2]=1.09017206e-1;
    w[3]=2.48105209e-2;
    w[4]=3.24377334e-3;
}

```

```

w[5]=2.28338636e-4;
w[6]=7.80255648e-6;
w[7]=1.08606937e-7;
w[8]=4.39934099e-10;
w[9]=2.22939365e-13;

```

```

t[0]=0.245340708;
t[1]=0.737473729;
t[2]=1.23407622;
t[3]=1.73853771;
t[4]=2.25497400;
t[5]=2.78880606;
t[6]=3.34785457;
t[7]=3.94476404;
t[8]=4.60368245;
t[9]=5.38748089;

```

```

if ((y<1.0 && x<4.0) || (y<1.8/(x+1.0) && x>4.0) )
    v=k1(x,y);
else if (y<2.5 && x<4.0)
    v=k2(x,y);
else
    v=k3(x,y);

```

```

return v;

```

```

}

```

```

/*****

```

```

Section:          k1
Type:             function
Date:            30 October 1990

```

```

Description:     This section does the actual voigt profile calculation
                 over the range y<1.0,x<4;y<1.8/(x+1),x>4. It uses the
                 Hummer-Faddeyeva/Terent'ev power series in y method.

```

```

*****/

```

```

double k1(double x, double y)

```

```

{

```

```

    double y2;
    double u1;
    double c[34],coef,bno1,bno2,bn,x1,f,funct,q,yn,dn,g;
    double dno1,dno2;
    int      i,ii;

```

```

    y2=pow(y,2);

```

```

    if ((pow(x,2)-y2) > 70.0)

```

```

    {
        u1=0.0;
    }

```

```

    else
        u1=exp(-pow(x,2)+y2)*cos(2.0*x*y);

```

```

    if (x > 5.0)

```

```

    {
        dno1=-(.5/pow(x,2)+.75/pow(x,4)+1.875/pow(x,6)+6.5625/pow(x,8)+
              29.53125/pow(x,10)+1162.4218/pow(x,12)+1055.7421/pow(x,14));
        dno2=(1.0-dno1)/(2.0*x);
    }

```

```

    else

```

```

    {

```

```

        /* Calculating Dawsons function from Hummers Chebyshev
           coefficients */

```

```

        c[0]=.1999999999972224;
        c[1]=-0.1840000000029998;
        c[2]=-0.1558399999965025;

```

```

c[3]=-.1216640000043988;
c[4]=.0877081599940391;
c[5]=-.0585141248086907;
c[6]=.0362157301623914;
c[7]=-.0208497654398036;
c[8]=.0111960116346270;
c[9]=-.56231896167109e-2;
c[10]=.26487634172265e-2;
c[11]=-.11732670757704e-2;
c[12]=.4899519978088e-3;
c[13]=-.1933630801528e-3;
c[14]=.722877446788e-4;
c[15]=-.256555124979e-4;
c[16]=.86620736841e-5;
c[17]=-.27876379719e-5;
c[18]=.8566873627e-6;
c[19]=-.2518433784e-6;
c[20]=.709360221e-7;
c[21]=-.191732257e-7;
c[22]=.49801256e-8;
c[23]=-.12447734e-8;
c[24]=.2997777e-9;
c[25]=-.696450e-10;
c[26]=.156262e-10;
c[27]=-.33897e-11;
c[28]=.7116e-12;
c[29]=-.1447e-12;
c[30]=.285e-13;
c[31]=-.55e-14;
c[32]=.10e-14;
c[33]=-.2e-15;

/* Chenshaws algorithm as given by Hummer */
bno1=0.0;
bno2=0.0;
x1=x/5.0;
coef=4.0*pow(x1,2)-2.0;
for (i=33;i>=0;i--)
(
    bn=coef*bno1-bno2+c[i];
    bno2=bno1;
    bno1=bn;
)
f=x1*(bn-bno2);
dno1=1.0-2.0*x*f;
dno2=f;

)
funct=y*dno1;
if (y < 1.0e-8)
(
    return ul-1.12837917*funct;
)
else
(
    q=1.0;
    yn=y;
    for (i=2;i<=50;i++)
    (
        dn=(x*dno1+dno2)*(-2.0)/(double)i;
        dno2=dno1;
        dno1=dn;
        if (fmod(i,2)!=0.0)
        (
            q=-q;
            yn=yn*y2;
            g=dn*yn;
            funct=funct+q*g;

```

```

        if (fabs(g/funct) < 1.0e-8)
        {
            return u1-1.12837917*funct;
        }
    }
}

```

```

}

/*****
Section:          k2
Type:            function
Date:            30 October 1990
Description:     This section does the actual voigt profile calculation
                 over the range 1.0<y<=2.5, x<=4. It uses a 20-term
                 Gauss-Hermite integration of K(x,y) as modified by
                 integration by parts.
*****/

```

```

double k2(double x, double y)
{
    double      y2;
    double g;
    double r,s;
    int         i;

    y2=pow(y,2);
    g=0.0;

    for (i=0;i<10;i++)
    {
        r=t[i]-x;
        s=t[i]+x;
        g=g+(4.0*pow(t[i],2)-2.0)*(r*atan2(r,y)+s*atan2(s,y)-0.5*y*
            (log(y2+pow(r,2))+log(y2+pow(s,2))))*w[i];
    }

    return 0.318309886*g;
}

```

```

/*****
Section:          k3
Type:            function
Date:            30 October 1990
Description:     This section does the actual voigt profile calculation
                 over the range y>=2.5,x<4;y>=1.8/(x+1),x>4. It uses a
                 20-term Gauss-Hermite integration of the original voigt
                 representation of K(x,y).
*****/

```

```

double k3(double x, double y)
{
    double y2;
    double g;
    int     i;

    y2=pow(y,2);
    g=0.0;

    for (i=0;i<10;i++)
    {
        g=g+(1.0/(pow((x-t[i]),2)+y2)+1.0/(pow((x+t[i]),2)+y2))*w[i];
    }

    return 0.318309886*y*g;
}

```

Appendix B. Tabulated Curves of Growth Data

The following data set is a sample of the "curves of growth" data produced by the program listed in Appendix A. This data is presented to aid future users of this code in the testing of their versions or modifications. The data presented represents a wide range of values for a , $a=0$ to 10. The " a " values typically used in the experiment in the flames studied here were ≈ 0.02 .

Sample Tabulated Curves of Growth Data

$\ln\left(\frac{K_J \cdot J \cdot 1.2 \sqrt{\ln 2}}{\Delta W_D \sqrt{\pi}}\right)$	$\ln\left(\frac{W_J \cdot J \cdot \sqrt{\ln 2}}{\Delta W_D}\right)$				
	a=0.00	a=0.02	a=0.10	a=1.00	a=10.00
-9.21034	-9.33116	-9.33122	-9.33147	-9.33432	-9.36345
-8.51719	-8.63805	-8.63811	-8.63835	-8.64119	-8.67030
-8.11173	-8.23262	-8.23268	-8.23292	-8.23573	-8.26484
-7.82405	-7.94497	-7.94503	-7.94527	-7.94806	-7.97716
-7.60090	-7.72186	-7.72192	-7.72216	-7.72493	-7.75401
-7.41858	-7.53958	-7.53963	-7.53986	-7.54262	-7.57169
-7.26443	-7.38546	-7.38552	-7.38574	-7.38848	-7.41754
-7.13090	-7.25196	-7.25202	-7.25224	-7.25497	-7.28402
-7.01312	-7.13422	-7.13427	-7.13449	-7.13719	-7.16623
-6.90776	-7.02889	-7.02894	-7.02916	-7.03184	-7.06087
-6.21461	-6.33610	-6.33614	-6.33632	-6.33882	-6.36774
-5.80914	-5.93099	-5.93102	-5.93115	-5.93347	-5.96229
-5.52146	-5.64366	-5.64368	-5.64378	-5.64591	-5.67462
-5.29832	-5.42087	-5.42088	-5.42094	-5.42288	-5.45149
-5.11600	-5.23890	-5.23890	-5.23892	-5.24068	-5.26919
-4.96185	-5.08510	-5.08509	-5.08507	-5.08665	-5.11505
-4.82831	-4.95192	-4.95190	-4.95184	-4.95324	-4.98153
-4.71053	-4.83449	-4.83446	-4.83436	-4.83557	-4.86377
-4.60517	-4.72949	-4.72944	-4.72930	-4.73033	-4.75842
-3.91202	-4.03986	-4.03971	-4.03919	-4.03838	-4.06542
-3.50656	-3.63792	-3.63765	-3.63674	-3.63410	-3.66010
-3.21888	-3.35375	-3.35337	-3.35208	-3.34761	-3.37256
-2.99573	-3.13411	-3.13363	-3.13194	-3.12565	-3.14956
-2.81341	-2.95529	-2.95470	-2.95263	-2.94451	-2.96739
-2.65926	-2.80463	-2.80393	-2.80148	-2.79155	-2.81338
-2.52573	-2.67458	-2.67377	-2.67094	-2.65920	-2.68000
-2.40795	-2.56028	-2.55936	-2.55615	-2.54260	-2.56236
-2.30259	-2.45839	-2.45737	-2.45377	-2.43842	-2.45714
-1.60944	-1.79959	-1.79751	-1.79016	-1.75701	-1.76544
-1.20397	-1.42783	-1.42471	-1.41370	-1.36317	-1.36143
-0.91629	-1.17320	-1.16908	-1.15449	-1.08698	-1.07519
-0.69315	-0.98248	-0.97737	-0.95930	-0.87522	-0.85349
-0.51083	-0.83195	-0.82588	-0.80441	-0.70416	-0.67261
-0.35668	-0.70898	-0.70197	-0.67719	-0.56116	-0.51990
-0.22314	-0.60603	-0.59810	-0.57009	-0.43866	-0.38781
-0.10536	-0.51823	-0.50941	-0.47825	-0.33179	-0.27146
0.00000	-0.44228	-0.43258	-0.39835	-0.23723	-0.16754
0.69315	-0.01375	0.00362	0.06467	0.35385	0.51137
1.09861	0.17289	0.19642	0.27860	0.66729	0.90279
1.38629	0.27753	0.30618	0.40550	0.87187	1.17662
1.60944	0.34527	0.37835	0.49206	1.01979	1.38609
1.79176	0.39357	0.43061	0.55683	1.13382	1.55492
1.94591	0.43040	0.47108	0.60848	1.22575	1.69577
2.07944	0.45985	0.50395	0.65155	1.30239	1.81617
2.19723	0.48423	0.53156	0.68861	1.36794	1.92101
2.30259	0.50493	0.55536	0.72127	1.42515	2.01359
2.99573	0.62155	0.69865	0.93420	1.78045	2.58793
3.40120	0.67829	0.77793	1.06468	1.98070	2.88916
3.68888	0.71480	0.83469	1.16256	2.12185	3.08495
3.91202	0.74132	0.87990	1.24216	2.23110	3.22656
4.09435	0.76196	0.91801	1.30977	2.32025	3.33605
4.24850	0.77874	0.95131	1.36878	2.39555	3.42468
4.38203	0.79283	0.98109	1.42128	2.46073	3.49885
4.49981	0.80492	1.00818	1.46863	2.51818	3.56250
4.60517	0.81549	1.03313	1.51180	2.56953	3.61818

Appendix C. Sample Calculation for the OH Radical in a CH₄/N₂O Flame

This Appendix demonstrates a sample calculation for converting integrated absorption profiles obtained from absorption spectroscopy to absolute concentrations of free radical species in flames. All values, unless otherwise specified, were taken from Lucht *et al.* [Ref. 1]. The equation numbers referenced are from the main body of the present report.

In this experiment, multiple scans over single absorption lines were performed. The integrated areas for these individual trials were calculated, then an average area was determined. It was this average area which was used in the calculations. For OH, the average integrated absorption for the Q₁(6) transition was experimentally determined to be:

$$W_{J''J'} [Q_1(6)] = 0.0842 \text{ cm}^{-1}$$

It is generally assumed that the line broadening parameter, *a*, is proportional to pressure and inversely proportional to temperature:

$$a \propto \frac{P}{T}$$

Lucht *et al.* have fit experimental data to this function and have found that:

$$a = 600 \frac{P}{T} \text{ for the OH radical}$$

where the units of *P* and *T* are atmospheres and Kelvin, respectively. All the flames in this study were run at 63 Torr (0.0829 atm). The integrated absorption of OH in the CH₄/N₂O flame was measured at 6.0 mm from the burner surface, where the temperature is 2600 K [Ref. 2]. Therefore:

$$\begin{aligned} a &= 0.01913 \\ P &= 0.0829 \text{ atm} \\ T &= 2600 \text{ K} \\ l &= 1.9 \text{ cm} \end{aligned}$$

To find the number density *N*₁₍₆₎ of the *N*'' = 6, *J*'' = 6.5, rotational level and the total OH number density *N*_{OH}.

For the OH²Π(*v*=0) ground electronic state (from Lucht *et al.*):

$$\begin{aligned} T_e &= 0 \\ G(v) &= 1841.9 \text{ cm}^{-1} \end{aligned}$$

For the Q₁(6) transition:

$$\begin{aligned} F_1(6) &= 768.1 \text{ cm}^{-1} \\ S_{J''J'} &= 12.66 \\ T_{J''J'} &= 0.969 \\ f_{00} &= 0.00096 \\ \omega_0 &= 32381 \text{ cm}^{-1} \end{aligned}$$

The Doppler half width $\Delta\omega_D$ for OH at 2600 K is defined by:

$$\Delta\omega_D = 2 \left(\frac{2kT \ln 2}{m_{OH} c^2} \right)^{\frac{1}{2}} \omega_0 = 0.2877 \text{ cm}^{-1} \quad (1)$$

where m_{OH} , the mass of OH, is 2.8×10^{-26} kg. α is defined as:

$$\alpha = \ln \left(\frac{W_{J''J'} \sqrt{\ln 2}}{\Delta\omega_D} \right) = -1.412 \quad (2)$$

which corresponds to the y-axis of the "curves of growth" plot. By graphically interpolating this value α for $a=0.01913$, β corresponds to the x-axis value, or:

$$\beta = \ln \left(\frac{K_{J''J'} \sqrt{\ln 2}}{\Delta\omega_D \sqrt{\pi}} \right) = -1.190 \quad (3)$$

By rearranging this equation to solve for $K_{J''J'}$

$$K_{J''J'} = \frac{\Delta\omega_D \sqrt{\pi}}{2 \sqrt{\ln 2}} e^{\beta} = 0.0490 \text{ cm}^{-2}. \quad (4)$$

Substituting this value for $K_{J''J'}$ into Equation 15 from the text to solve for the number density for the $Q_1(6)$ line, using $\frac{m_e c^2}{\pi e^2} = 1.133 \times 10^{12} \text{ cm}^{-1}$.

$$N_1(6) = N_{J''} = \frac{m_e c^2}{\pi e^2} \frac{K_{J''J'}}{f_{v''v'} S_{J''J'} T_{J''J'}} = 6.603 \times 10^{13} \text{ cm}^{-3}. \quad (5)$$

We can relate this number to the overall number density of OH by using Equation 16 and Q_e , Q_v , Q_r equal to 4, 0.360, and 97.52, respectively, from Equations 17-19.

$$N_{OH} = N_{J''} \frac{Q_e Q_v Q_r}{2J''+1} \exp\left(\frac{hc}{kT} [T_e(n) + G(v) + F(J'')]\right) = 2.815 \times 10^{15} \text{ cm}^{-3}. \quad (6)$$

This is the final OH number density. It can be converted into mole fraction using the following formula:

$$\text{Mole fraction}_{OH} = y_{OH} = \frac{N_{OH}}{\text{Total Number Density at 63 Torr and 2600 K}} = \frac{2.815 \times 10^{15}}{2.337 \times 10^{17}} = 0.01202. \quad (7)$$